(Preprint) AAS 16-045

FAST KALMAN FILTERING FOR RELATIVE SPACECRAFT POSITION AND ATTITUDE ESTIMATION FOR THE RAVEN ISS HOSTED PAYLOAD

Joseph M Galante[*], John Van Eepoel[†], Chris D'Souza[‡], and Bryan Patrick[§]

The Raven ISS Hosted Payload will feature several pose measurement sensors on a pan/tilt gimbal which will be used to autonomously track resupply vehicles as they approach and depart the International Space Station. This paper discusses the derivation of a Relative Navigation Filter (RNF) to fuse measurements from the different pose measurement sensors to produce relative position and attitude estimates. The RNF relies on relative translation and orientation kinematics and careful pose sensor modeling to eliminate dependence on orbital position information and associated orbital dynamics models. The filter state is augmented with sensor biases to provide a mechanism for the filter to estimate and mitigate the offset between the measurements from different pose sensors.

INTRODUCTION

There is significant need for and interest in the design of estimation filters used for relative navigation during rendezvous and docking between spacecraft. A particularly challenging version of this problem is when the spacecraft to be tracked does not have cooperative navigation aids such as laser retroreflectors, visual fiducials, or radiometric relays. In this situation, the "chaser" spacecraft must use optical sensors such as visual cameras, infrared cameras, or LIDAR systems to sense the outer "skin" of the spacecraft to be tracked to provide measurements of the relative position and orientation. At the present state of optical sensor technology, these sensors each have their own advantages and disadvantages: visual cameras are high resolution but are very sensitive to lighting conditions, infrared cameras are robust to lighting conditions but spacecraft are difficult to model in the infrared spectrum and infrared cameras may not function with bright objects in the field of view, and LIDAR cameras are robust to lighting conditions but have limited resolution. To build a reliable relative navigation system, it is desirable to fuse the measurements of several different types of sensors in one navigation filter.

While fusing the solutions of disparate sensor measurements is challenging enough, the estimation problem for relative spacecraft navigation during rendezvous and docking is placed under further constraints by

[*] Aerospace Engineer, NASA Goddard Space Flight Center, Attitude Control and Estimation Systems Branch, Greenbelt, MD 20771. email: joseph.m.galante@nasa.gov.

[†] Aerospace Engineer, NASA Goddard Space Flight Center, Attitude Control and Estimation Systems Branch, Greenbelt, MD 20771. email: john.m.vaneepoel@nasa.gov.

[‡] Deputy Branch Chief, NASA Johnson Space Center, GN&C Autonomous Flight Systems Branch Branch, Houston, TX 77058. email: chris.dsouza-1@nasa.gov.

[§] Senior GNC Engineer, Emergent Space Technologies, 6411 Ivy Lane, Greenbelt, MD 20770. email: bryan.a.patrick@nasa.gov.

the dynamics of the system. The purpose of the estimation filter is to provide a relative navigation solution to the control system. Specifically, the control system may require estimates from the navigation filter at a sample rate that is much higher than what the optical camera systems can provide. It may also be important that the navigation system account for the angular velocity of both spacecraft.

To develop relative navigation technology capable of meeting these objectives, NASA has built the Raven technology demonstration payload which is to be installed on the International Space Station in the summer of 2016 as part of the United States' Department of Defense's Space Technology Program (STP-H5). Raven consists of a visual camera, infrared camera, and flash LIDAR mounted on a pan/tilt gimbal that will allow for observation of resupply vehicles as they approach and depart the ISS. Note that the ISS does not directly measure the relative position, velocity, attitude, or angular rate of resupply vehicles. Currently, resupply vehicles must feature their own rendezvous sensor suite to provide a relative navigation solution which ISS Mission Control and ISS crew members monitor. This operational arrangement means that resupply vehicles are not outfitted with laser retroreflectors or optical fiducials, making ISS resupply vehicles excellent candidates to test relative navigation sensors and algorithms. Furthermore, the Raven technology demonstration represents a prototype of a new rendezvous paradigm; much like air traffic control utilizes their own radar systems to maintain operational awareness of their local air space, a relative navigation sensor suite like Raven would allow the ISS to maintain independent operational awareness of its local space. An ISS relative navigation sensor suite may also enable cheaper and less complicated resupply vehicles by offloading the sensing and computational burden from the visiting vehicles.

There has been a great amount of activity in the relative pose estimation literature. Kim[1] developed a Multiplicative Extended Kalman Filter (MEKF)[2,3,4] to estimate a relative pose state using line-of-sight (LOS) measurements, but did not directly account for chaser rotation in the filter.[5] Woffinden[6] developed an MEKF to estimate the absolute states of two spacecraft using LOS measurements. Most of these approaches incorporate some form of orbital dynamics[1,6,7,8,9,10,11,5] which requires orbital position information from GPS measurements and may involve computationally expensive gravity and drag model evaluations to be sufficiently accurate. None of these listed approaches explicitly mitigate the situation of differing solutions from different pose measurement sensors, nor are they designed to accept pose measurements.

Our approach to this problem is more like that of Tweddle[12] which utilizes pose measurements and kinematics exclusively; specifically, no orbital dynamics are considered. Raven's cameras and image processing algorithms are able to provide pose measurements rapidly. Raven does not have access to orbital position information in real time. Given these constraints, the design of the Raven relative navigation filter (RNF) focuses on careful modeling of the sensor dynamics the relative kinematics. Our approach differs from that of Tweddle[12] in that Tweddle does not explicitly account for chaser rotation[5] nor does Tweddle provide a mechanism to mitigate disagreement amongst pose solutions.

MATHEMATICAL PRELIMINARIES

To acclimate the reader to our notation, we provide a brief overview of some of the mathematical concepts used to describe the kinematics of rotating rigid bodies. We denote a position vector from a point D to a point E as $\vec{\boldsymbol{r}}_{E/D}$. Note that the vector $\vec{\boldsymbol{r}}_{E/D}$ is a geometric construct indicating magnitude and direction but does not have a unique numeric representation. Consider a reference frame $\mathcal{F}_A$ defined by an origin point O_A and three pairwise-orthogonal unit vectors $\vec{\boldsymbol{a}}_x$, $\vec{\boldsymbol{a}}_y$, and $\vec{\boldsymbol{a}}_z$ (which of course satisfy the right hand rules

$\vec{a}_x \times \vec{a}_y = \vec{a}_z$, $\vec{a}_y \times \vec{a}_z = \vec{a}_x$, and $\vec{a}_z \times \vec{a}_x = \vec{a}_y$). The position vector $\vec{r}_{E/D}$ can then be resolved as coordinates along the axes defining reference frame $\mathcal{F}_A$. We organize the resulting coordinates as a column matrix defined as follows:

$$\boldsymbol{r}^{A}_{E/D} = \begin{bmatrix} \vec{r}_{E/D} \bullet \vec{a}_x \\ \vec{r}_{E/D} \bullet \vec{a}_y \\ \vec{r}_{E/D} \bullet \vec{a}_z \end{bmatrix} \tag{1}$$

We notate the cross product between two column matrices $\boldsymbol{a}, \boldsymbol{b} \in \mathbb{R}^{3\times 1}$ in any of the following ways:

$$\boldsymbol{a} \times \boldsymbol{b} = \begin{bmatrix} a_x \\ a_y \\ a_z \end{bmatrix} \times \begin{bmatrix} b_x \\ b_y \\ b_z \end{bmatrix} = \begin{bmatrix} 0 & -a_z & a_y \\ a_z & 0 & -a_x \\ -a_y & a_x & 0 \end{bmatrix} \begin{bmatrix} b_x \\ b_y \\ b_z \end{bmatrix} = \Big[\boldsymbol{a} \times\Big] \boldsymbol{b} \tag{2}$$

The orientation of reference frame $\mathcal{F}_B$ relative to frame $\mathcal{F}_A$ can be described using a rotation matrix which we notate as $R_{B/A}$. The rotation matrix can be understood as an operator which can be used to switch the frame of expression:

$$\boldsymbol{r}^{B}_{E/D} = R_{B/A} \boldsymbol{r}^{A}_{E/D} \tag{3}$$

While we regard the rotation matrix as the fundamental description of orientation, it is cumbersome to work with as it consists of nine numbers which satisfy six constraints. The rotation matrix may be parameterized by a unit quaternion which only consists of four numbers, the minimum required for a global nonsingular orientation parameterization:[13]

$$\boldsymbol{r}^{B}_{E/D} = R\left(\boldsymbol{q}_{B/A}\right) \boldsymbol{r}^{A}_{E/D} = R\left(\begin{bmatrix} \boldsymbol{\epsilon} \\ \eta \end{bmatrix}\right) \boldsymbol{r}^{A}_{E/D} = \left((\eta^2 - \boldsymbol{\epsilon}^T \boldsymbol{\epsilon}) \mathbb{I}_{3\times 3} - 2\eta \left[\boldsymbol{\epsilon} \times\right] + 2\boldsymbol{\epsilon}\boldsymbol{\epsilon}^T\right) \boldsymbol{r}^{A}_{E/D} \tag{4}$$

where $\mathbb{I}_{3\times 3}$ is the 3×3 identity matrix. The components of a unit quaternion are frequently described[14,15] in terms of the Euler axis $\boldsymbol{e}$ and Euler angle ϕ which we denote as

$$\boldsymbol{q} = \begin{bmatrix} \boldsymbol{\epsilon} \\ \eta \end{bmatrix} = \begin{bmatrix} \boldsymbol{e} \sin\left(\frac{\phi}{2}\right) \\ \cos\left(\frac{\phi}{2}\right) \end{bmatrix} \tag{5}$$

The construction of a rotation matrix given a unit quaternion is more involved, but a robust solution is given by Markley.[16]

We use the following quaternion multiplication rule:[4]

$$\boldsymbol{q} \otimes \boldsymbol{p} = \begin{bmatrix} \boldsymbol{\epsilon}_q \\ \eta_q \end{bmatrix} \otimes \begin{bmatrix} \boldsymbol{\epsilon}_p \\ \eta_p \end{bmatrix} = [\boldsymbol{q} \otimes] \boldsymbol{p} = \begin{bmatrix} \eta_q \mathbb{I}_{3\times 3} - \left[\boldsymbol{\epsilon}_q \times\right] & \boldsymbol{\epsilon}_q \\ -\boldsymbol{\epsilon}_q^T & \eta_q \end{bmatrix} \begin{bmatrix} \boldsymbol{\epsilon}_p \\ \eta_p \end{bmatrix} = \begin{bmatrix} \eta_q \boldsymbol{\epsilon}_p + \eta_p \boldsymbol{\epsilon}_q - \boldsymbol{\epsilon}_q \times \boldsymbol{\epsilon}_p \\ \eta_q \eta_p - \boldsymbol{\epsilon}_q^T \boldsymbol{\epsilon}_p \end{bmatrix} \tag{6}$$

The quaternion multiplication rule is defined such that for frames $\mathcal{F}_A$, $\mathcal{F}_B$, and $\mathcal{F}_C$:

$$\boldsymbol{r}_{E/D}^{C} = R_{C/A}\,\boldsymbol{r}_{E/D}^{A} = R\left(\boldsymbol{q}_{C/A}\right)\boldsymbol{r}_{E/D}^{A} = R\left(\boldsymbol{q}_{C/B} \otimes \boldsymbol{q}_{B/A}\right)\boldsymbol{r}_{E/D}^{A} \tag{7}$$

We further overload the quaternion multiplication rule to allow for multiplication of 4×1 quaternions, such as $\boldsymbol{q} = \begin{bmatrix} \boldsymbol{\epsilon} \\ \eta \end{bmatrix}$, with 3×1 column matrices, such as $\boldsymbol{\omega}$, using the following definitions:[4]

$$\boldsymbol{\omega} \otimes \boldsymbol{q} = \begin{bmatrix} \boldsymbol{\omega} \\ 0 \end{bmatrix} \otimes \boldsymbol{q} = [\boldsymbol{\omega} \otimes]\,\boldsymbol{q} = \begin{bmatrix} -[\boldsymbol{\omega} \times] & \boldsymbol{\omega} \\ -\boldsymbol{\omega}^{T} & 0 \end{bmatrix} \begin{bmatrix} \boldsymbol{\epsilon} \\ \eta \end{bmatrix} = \begin{bmatrix} \eta\,\boldsymbol{\omega} - \boldsymbol{\omega} \times \boldsymbol{\epsilon} \\ -\boldsymbol{\omega}^{T}\boldsymbol{\epsilon} \end{bmatrix} \tag{8}$$

$$\boldsymbol{q} \otimes \boldsymbol{\omega} = \boldsymbol{q} \otimes \begin{bmatrix} \boldsymbol{\omega} \\ 0 \end{bmatrix} = [\boldsymbol{q} \otimes]\,\boldsymbol{\omega} = \begin{bmatrix} \eta\mathbb{I}_{3\times 3} - [\boldsymbol{\epsilon} \times] & \boldsymbol{\epsilon} \\ -\boldsymbol{\epsilon}^{T} & \eta \end{bmatrix} \begin{bmatrix} \boldsymbol{\omega} \\ 0 \end{bmatrix} = \begin{bmatrix} \eta\,\boldsymbol{\omega} - \boldsymbol{\epsilon} \times \boldsymbol{\omega} \\ -\boldsymbol{\epsilon}^{T}\boldsymbol{\omega} \end{bmatrix} \tag{9}$$

Combining the overloaded quaternion multiplication rule with the change of frame expression of Equation 4 we find:

$$\boldsymbol{r}_{E/D}^{B} = R_{B/A}\,\boldsymbol{r}_{E/D}^{A} = \boldsymbol{q}_{B/A} \otimes \boldsymbol{r}_{E/D}^{A} \otimes \boldsymbol{q}_{B/A}^{-1} \tag{10}$$

where, for the unit quaternion $\boldsymbol{q}_{B/A} = \begin{bmatrix} \boldsymbol{\epsilon}_{B/A} \\ \eta_{B/A} \end{bmatrix}$,

$$\boldsymbol{q}_{B/A}^{-1} = \begin{bmatrix} -\boldsymbol{\epsilon}_{B/A} \\ \eta_{B/A} \end{bmatrix} \quad \text{or} \quad \begin{bmatrix} \boldsymbol{\epsilon}_{B/A} \\ -\eta_{B/A} \end{bmatrix} \tag{11}$$

is the inverse of the quaternion $\boldsymbol{q}_{B/A}$ and satisfies the property

$$R_{B/A}R_{B/A}^{-1} = R\left(\boldsymbol{q}_{B/A}\right)R\left(\boldsymbol{q}_{B/A}^{-1}\right) = R\left(\boldsymbol{q}_{B/A} \otimes \boldsymbol{q}_{B/A}^{-1}\right) = R\left(\boldsymbol{q}_{Identity}\right) = \mathbb{I}_{3\times 3} \tag{12}$$

Finally, we make frequent use of an orientation error parameterization. While many parameterizations exist,[3,17] we elect to use Gibb's Parameters (also known as Classic Rodrigues Parameters). The transformation from a unit quaternion $\boldsymbol{q} = \begin{bmatrix} \boldsymbol{\epsilon} \\ \eta \end{bmatrix} \in \mathbb{R}^{4\times 1}$ to Gibbs Parameters $\boldsymbol{g} \in \mathbb{R}^{3\times 1}$ is

$$\boldsymbol{g}\left(\boldsymbol{q}\right) = \frac{\boldsymbol{\epsilon}}{\eta} \tag{13}$$

while the inverse transformation is given by

$$\boldsymbol{q}\left(\boldsymbol{g}\right) = \frac{1}{\sqrt{1 + \boldsymbol{g}^{T}\boldsymbol{g}}} \begin{bmatrix} \boldsymbol{g} \\ 1 \end{bmatrix} \tag{14}$$

Note that the Gibbs parameterization is singular at maximum orientation difference (when $\eta = 0$).

SYSTEM DESCRIPTION

Raven is a technology demonstration payload scheduled to launch to the International Space Station (ISS) in summer 2016 as part of the US Air Force's Space Technology Program (STP-H5).[18] As shown in Figure 2, Raven consists of a visual light camera with motorized zoom lens, an infrared camera, and a flash LIDAR camera in a sensor enclosure. The sensor enclosure also contains a MEMS Inertial Measurement Unit (IMU). The sensor enclosure is attached to a baseplate through a two axis gimbal providing pan and tilt motion. The baseplate is rigidly attached to the ISS; it contains a SpaceCube 2.0 flight processing computer and associated electronics. The ISS provides a mount point, power supply, telemetry storage and downlink, and timing information, but no position or orientation information. Raven will have access to the telemetry from a quaternion output star tracker mounted near the baseplate.

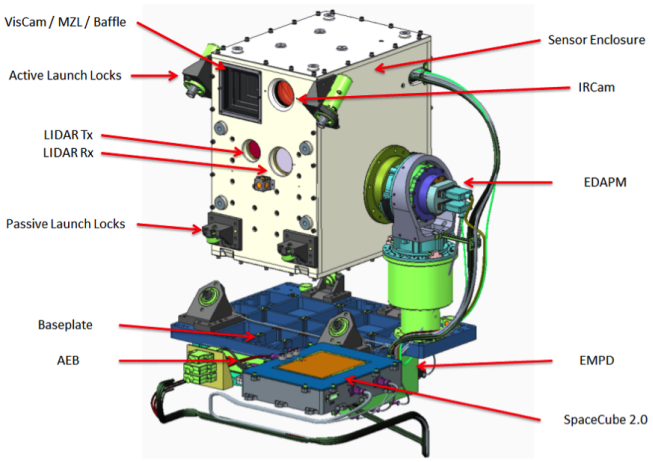

Figure 1. Computer rendering of the Raven payload.

Once installed and checked out, Raven's mission is to autonomously track ISS resupply vehicles (later referred to as visiting vehicles or VV for short). Note that while the ISS is designed to be looked at by visiting vehicles by hosting laser retroreflectors, visual fiducials, and radio telemetry (KURS), resupply vehicles such as the SpaceX Dragon, Orbital ATK's Cygnus, ESA's ATV, JAXA's HTV, and the Russian Progress and Soyuz vehicles do not. Furthermore, there are no plans for real-time information sharing between Raven and the visiting vehicles. In order for Raven to be able to maintain tracking of a visiting vehicles, it must be able to use its visible, infrared, and LIDAR cameras to detect the position and orientation of the visiting vehicle without cooperative aids such as retroreflectors or fiducials. To compound the challenge, visiting vehicles frequently pass between the Earth and the ISS during approach; thus any computer vision algorithms used must be robust to background clutter.

Raven will need to point its visual, infrared, and LIDAR cameras accurately to keep the visiting vehicle in the cameras' fields of view, but the Raven mount point is expected to be exposed to some disturbance vibrations. Raven will be mounted on an Express Logistics Carrier (ELC) on the port nadir side of the ISS in close proximity to the port solar array alpha rotation joint (SARJ). In addition to the vibrations introduced by the solar array rotation motors, the ISS is known to experience vibrations along its truss due to the

operation of numerous coolant pumps, air handling equipment, and crew activity. In order to actively cancel (or at least mitigate) the impact of these disturbances on the ability of Raven to maintain pointing at long relative ranges, the Raven Pointing Control System is designed to operate at 25 Hz.

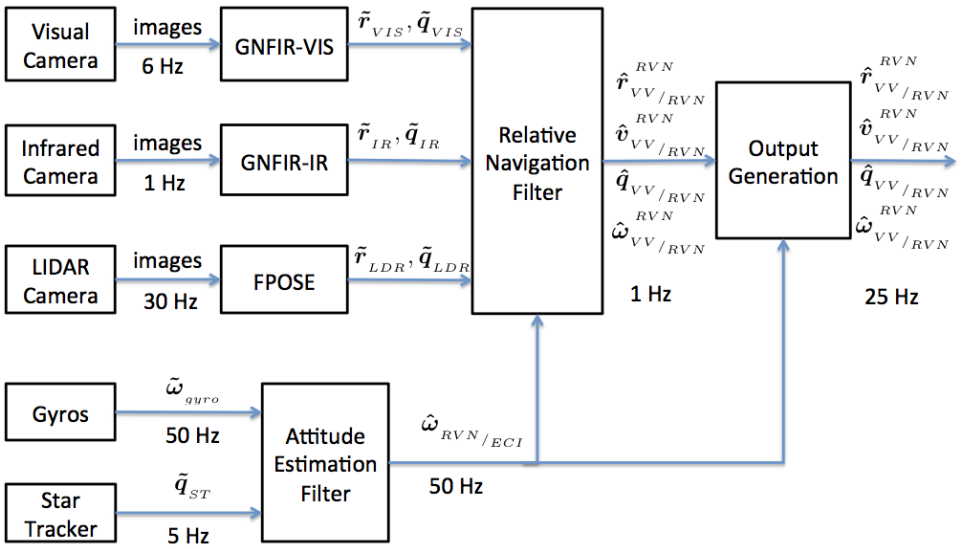

Figure 2. Raven estimation system block diagram. Sensor rates and vision algorithm output rates are approximate.

Relative position and orientation measurements are provided by vision algorithms that process images from the cameras. The visual and infrared imagery are processed by independent instantiations of the Goddard Natural Feature Image Recognition (GNFIR) application while the flash LIDAR camera's images are processed by the Goddard FlashPose (FPOSE) application. Both GNFIR and FPOSE have similar basics of operation: they use an a-priori generated 3D model of the visiting vehicle, they use an iterative algorithm to project the 3D model of the visiting vehicle onto the camera images, and use a least squares like minimization technique to refine relative pose estimates so that projected visiting vehicle model features match with features seen in the imagery. Both applications output measurements of relative pose, which we define as the translational position of the visiting vehicle relative to the camera $\tilde{r}^{RVN}_{VV/RVN}$ and the relative orientation of the visiting vehicle relative to the camera $\tilde{q}_{VV/RVN}$. GNFIR is based on the Drummond and Cippola technique[19] and has flight heritage.[20] FPOSE is based on the Besl and McKay technique.[21] The applications make extensive use of the processing capabilities of the SpaceCube 2.0 flight computer which features multiple embedded processors and FPGA fabric. The integration of FPGA hardware with the flight processors allow for significant hardware acceleration of the image processing algorithms, such as feature extraction. Both FPOSE and GNFIR pose measurements have significant cross-coupling between the translation and orientation components.[22]

The Raven sensor enclosure inertial angular rate $\hat{\omega}^{RVN}_{RVN/ECI}$ is estimated by an independent Attitude Estimation Filter. The Attitude Estimation Filter is a standard Multiplicative Extended Kalman Filter

(MEKF).[2,3] The MEKF uses low sample rate star tracker measurements and simple rigid body kinematics to estimate and mitigate gyro bias from the fast sample rate gyro. The Relative Navigation Filter (RNF), which is the focus of this paper, treats information from the Attitude Estimation Filter as perfect.The Output Generation block uses angular rate estimates from the Attitude Estimation Filter to propagate the RNF's estimate at 25 Hz for the Pointing Control System.

STATE DYNAMICS

The state for the Raven Relative Navigation Filter (RNF) is chosen to be the relative translational position, relative translational velocity, relative orientation, visiting vehicle inertial angular rate, and sensor biases.

$$\boldsymbol{X} = \begin{bmatrix} \boldsymbol{r}^{RVN}_{VV/RVN} \\ \boldsymbol{v}^{RVN}_{VV/RVN} \\ \boldsymbol{q}_{VV/RVN} \\ \boldsymbol{\omega}^{VV}_{VV/ECI} \\ \boldsymbol{b} \end{bmatrix} = \begin{bmatrix} \boldsymbol{r} \\ \boldsymbol{v} \\ \boldsymbol{q} \\ \boldsymbol{\omega} \\ \boldsymbol{b} \end{bmatrix} \tag{15}$$

where $\mathcal{F}_{VV}$ is a reference frame rigidly attached to the visiting vehicle, $\mathcal{F}_{RVN}$ is a reference frame rigidly attached to the Raven sensor enclosure, and $\mathcal{F}_{ECI}$ is an Earth-centered inertial reference frame.

Since Raven does not have real-time access to orbital position information, the RNF does not have enough information to deduce the local vertical local horizontal (LVLH) frame which precludes the RNF from utilizing Clohessy Wiltshire (CW) dynamics.[23] While it may seem disadvantageous to neglect orbital effects, the fast output rate of the relative pose measurements from the computer vision algorithms appear to be suitable for the expected benign relative motion dynamics during rendezvous and docking/berthing. In fact, by neglecting orbital dynamics, the RNF benefits from reduced system complexity as it doesn't rely on GPS or orbital information as well as reduced computational load necessary for orbit calculations (such as computation of the LVLH frame and orbit parameters for a CW filter,[1] or evaluation of high order gravity and air drag models for a filter with high fidelity orbital dynamics[24]).

The bias states include 18 elements, one for each sensor axis: three for GNFIR-VIS translation, three for GNFIR-VIS orientation, three for GNFIR-IR translation, and so on. The biases are assumed to each be independent first order Gauss Markov biases:

$$\begin{aligned} \dot{\boldsymbol{b}} &= -\text{diag}\left(\frac{1}{\tau_1}, \frac{1}{\tau_2}, \ldots, \frac{1}{\tau_{18}}\right)\boldsymbol{b} + W_b \boldsymbol{w}_b \\ &= -T\boldsymbol{b} + W_b \boldsymbol{w}_b \end{aligned} \tag{16}$$

where $\boldsymbol{w}_b \sim \mathcal{N}\left(\boldsymbol{0}, \mathbb{I}_{18\times 18}\right)$ is a zero mean unit variance Gauss white process scaled by the matrix W_b. The biases are sometimes referenced by the sensor to which they apply:

$$\boldsymbol{b}^T = \begin{bmatrix} \boldsymbol{b}^T_{VIS,tran} & \boldsymbol{b}^T_{VIS,rot} & \boldsymbol{b}^T_{IR,tran} & \boldsymbol{b}^T_{IR,rot} & \boldsymbol{b}^T_{LDR,tran} & \boldsymbol{b}^T_{LDR,rot} \end{bmatrix} \tag{17}$$

Relative Translation Dynamics

The translation dynamics follow directly from basic vector arithmetic and application of the transport theorem. The relative translation is given by:

$$\boldsymbol{r} = \boldsymbol{r}^{RVN}_{VV/RVN} = \boldsymbol{r}^{RVN}_{VV/ECI} - \boldsymbol{r}^{RVN}_{RVN/ECI} \tag{18}$$

Application of the transport theorem yields

$$\begin{aligned} {}^{ECI}\frac{d}{dt}\left(\boldsymbol{r}^{RVN}_{VV/RVN}\right) &= {}^{RVN}\frac{d}{dt}\left(\boldsymbol{r}^{RVN}_{VV/RVN}\right) + \boldsymbol{\omega}^{RVN}_{RVN/ECI} \times \boldsymbol{r}^{RVN}_{VV/RVN} \\ &= \boldsymbol{v} + \boldsymbol{\omega}^{RVN}_{RVN/ECI} \times \boldsymbol{r} \end{aligned} \tag{19}$$

A second application of the transport theorem yields

$$\begin{aligned} {}^{ECI}\frac{d}{dt}\left({}^{ECI}\frac{d}{dt}\left(\boldsymbol{r}^{RVN}_{VV/RVN}\right)\right) &= \dot{\boldsymbol{v}} + \boldsymbol{\alpha}^{RVN}_{RVN/ECI} \times \boldsymbol{r} + 2\boldsymbol{\omega}^{RVN}_{RVN/ECI} \times \boldsymbol{v} + \boldsymbol{\omega}^{RVN}_{RVN/ECI} \times \left(\boldsymbol{\omega}^{RVN}_{RVN/ECI} \times \boldsymbol{r}\right) \\ &\approx \dot{\boldsymbol{v}} + 2\boldsymbol{\omega}^{RVN}_{RVN/ECI} \times \boldsymbol{v} \end{aligned} \tag{20}$$

where we have made the simplifying assumptions that $\boldsymbol{\omega}^{RVN}_{RVN/ECI}$ has negligible change over the filter update interval (implying $\boldsymbol{\alpha}^{RVN}_{RVN/ECI} \approx \mathbf{0}$) and that the triple product term $\boldsymbol{\omega}^{RVN}_{RVN/ECI} \times \left(\boldsymbol{\omega}^{RVN}_{RVN/ECI} \times \boldsymbol{r}\right)$ is insignificant.

Of course, the relative acceleration can also be evaluated using Newton's second law:

$$\begin{aligned} {}^{ECI}\frac{d}{dt}\left({}^{ECI}\frac{d}{dt}\left(\boldsymbol{r}^{RVN}_{VV/RVN}\right)\right) &= \frac{1}{m_{VV}}\boldsymbol{F}_{VV} - \frac{1}{m_{ISS}}\boldsymbol{F}_{ISS} \\ &\approx W_{tran}\boldsymbol{w}_{tran} \end{aligned} \tag{21}$$

where the unknown disturbance accelerations and orbital dynamics accelerations are modeled as a unit variance zero mean Gaussian noise process $\boldsymbol{w}_{tran} \sim \mathcal{N}\left(\mathbf{0}, \mathbb{I}_{3\times 3}\right)$ scaled by a positive definite matrix W_{tran}.

Combining the kinematic relationship of Equation 20 with the application of Newton's law in Equation 21 yields the relation for the dynamics of the velocity state:

$$\dot{\boldsymbol{v}} \approx -2\boldsymbol{\omega}^{RVN}_{RVN/ECI} \times \boldsymbol{v} + W_{tran}\boldsymbol{w}_{tran} \tag{22}$$

Relative Rotation Dynamics

The rotational kinematic equation for a rigid body expressed for a quaternion parameterization is known to be[4]

$$\dot{\boldsymbol{q}}_{VV/ECI} = \frac{1}{2}\boldsymbol{\omega}^{VV}_{VV/ECI} \otimes \boldsymbol{q}_{VV/ECI} \tag{23}$$

when expressed for the visiting vehicle, for the Raven sensor enclosure, is similarly

$$\dot{\boldsymbol{q}}_{_{RVN/_{ECI}}} = \frac{1}{2}\boldsymbol{\omega}^{RVN}_{_{RVN/_{ECI}}} \otimes \boldsymbol{q}_{_{RVN/_{ECI}}} \tag{24}$$

The relative quaternion is given by

$$\boldsymbol{q}_{_{VV/_{RVN}}} = \boldsymbol{q}_{_{VV/_{ECI}}} \otimes \boldsymbol{q}^{-1}_{_{RVN/_{ECI}}} \tag{25}$$

Taking the derivative of the relative quaternion, we find:

$$\dot{\boldsymbol{q}}_{_{VV/_{RVN}}} = \dot{\boldsymbol{q}}_{_{VV/_{ECI}}} \otimes \boldsymbol{q}^{-1}_{_{RVN/_{ECI}}} + \boldsymbol{q}_{_{VV/_{ECI}}} \otimes \frac{d}{dt}\left(\boldsymbol{q}^{-1}_{_{RVN/_{ECI}}}\right) \tag{26}$$

A relation for $\frac{d}{dt}\left(\boldsymbol{q}^{-1}_{_{RVN/_{ECI}}}\right)$ can be found by taking the derivative of $\boldsymbol{q}_{_{RVN/_{ECI}}} \otimes \boldsymbol{q}^{-1}_{_{RVN/_{ECI}}} = \boldsymbol{q}_{_{Identity}}$:

$$\begin{aligned} \dot{\boldsymbol{q}}_{_{RVN/_{ECI}}} \otimes \boldsymbol{q}^{-1}_{_{RVN/_{ECI}}} + \boldsymbol{q}_{_{RVN/_{ECI}}} \otimes \frac{d}{dt}\left(\boldsymbol{q}^{-1}_{_{RVN/_{ECI}}}\right) &= \boldsymbol{0} \\ \frac{d}{dt}\left(\boldsymbol{q}^{-1}_{_{RVN/_{ECI}}}\right) &= -\frac{1}{2}\boldsymbol{q}^{-1}_{_{RVN/_{ECI}}} \otimes \boldsymbol{\omega}^{RVN}_{_{RVN/_{ECI}}} \end{aligned} \tag{27}$$

Combining Equations 26, 23, and 27 leads to:

$$\begin{aligned} \dot{\boldsymbol{q}}_{_{VV/_{RVN}}} &= \dot{\boldsymbol{q}}_{_{VV/_{ECI}}} \otimes \boldsymbol{q}^{-1}_{_{RVN/_{ECI}}} + \boldsymbol{q}_{_{VV/_{ECI}}} \otimes \frac{d}{dt}\left(\boldsymbol{q}^{-1}_{_{RVN/_{ECI}}}\right) \\ &= \frac{1}{2}\boldsymbol{\omega}^{VV}_{_{VV/_{ECI}}} \otimes \boldsymbol{q}_{_{VV/_{ECI}}} \otimes \boldsymbol{q}^{-1}_{_{RVN/_{ECI}}} - \frac{1}{2}\boldsymbol{q}_{_{VV/_{ECI}}} \otimes \boldsymbol{q}^{-1}_{_{RVN/_{ECI}}} \otimes \boldsymbol{\omega}^{RVN}_{_{RVN/_{ECI}}} \\ &= \frac{1}{2}\boldsymbol{\omega}^{VV}_{_{VV/_{ECI}}} \otimes \boldsymbol{q}_{_{VV/_{RVN}}} - \frac{1}{2}\boldsymbol{q}_{_{VV/_{RVN}}} \otimes \boldsymbol{\omega}^{RVN}_{_{RVN/_{ECI}}} \qquad (28) \\ &= \frac{1}{2}\boldsymbol{\omega}^{VV}_{_{VV/_{ECI}}} \otimes \boldsymbol{q}_{_{VV/_{RVN}}} - \frac{1}{2}\boldsymbol{q}_{_{VV/_{RVN}}} \otimes \boldsymbol{q}^{-1}_{_{VV/_{RVN}}} \otimes \boldsymbol{\omega}^{VV}_{_{RVN/_{ECI}}} \otimes \boldsymbol{q}_{_{VV/_{RVN}}} \\ &= \frac{1}{2}\left(\boldsymbol{\omega}^{VV}_{_{VV/_{ECI}}} - \boldsymbol{\omega}^{VV}_{_{RVN/_{ECI}}}\right) \otimes \boldsymbol{q}_{_{VV/_{RVN}}} \\ &= \frac{1}{2}\boldsymbol{\omega}^{VV}_{_{VV/_{RVN}}} \otimes \boldsymbol{q}_{_{VV/_{RVN}}} \qquad (29) \end{aligned}$$

Either Equation 28 or Equation 29 can be used for the design of the RNF. Equation 29 is used for the full state propagation, while Equation 28 is used to design the linearized error state dynamics.

The rotation dynamics follow from the Euler-Newton equation for a rigid body:

$${}^{ECI}\frac{d}{dt}\boldsymbol{\omega}^{VV}_{_{VV/_{ECI}}} = J^{-1}\left(\left(J\boldsymbol{\omega}^{VV}_{_{VV/_{ECI}}}\right) \times \boldsymbol{\omega}^{VV}_{_{VV/_{ECI}}}\right) + W_{_{rot}}\boldsymbol{w}_{_{rot}} \tag{30}$$

where the unknown disturbance angular accelerations are modeled as a unit variance zero mean Gaussian noise process $\boldsymbol{w}_{_{rot}} \sim \mathcal{N}\left(\boldsymbol{0}, \mathbb{I}_{_{3\times 3}}\right)$ scaled by a positive definite matrix $W_{_{rot}}$ and J is the inertia tensor of the visiting vehicle.

State Propagation Equations

The RNF may propagate the state estimates by taking the expectation of the above dynamics relations and integrating over the propagation interval. Assuming angular rates and translational velocities are constant over the filter propagation interval, we find:

$$\begin{aligned}
\hat{\boldsymbol{r}}_{k} &= \hat{\boldsymbol{r}}_{k-1} + \Delta t \hat{\boldsymbol{v}}_{k-1} \\
\hat{\boldsymbol{v}}_{k} &= \hat{\boldsymbol{v}}_{k-1} - 2\Delta t \hat{\boldsymbol{\omega}}^{RVN}_{RVN/ECI,k-1} \times \hat{\boldsymbol{v}}_{k-1} \\
\hat{\boldsymbol{q}}_{k} &= \left[\cos\left(\frac{\Delta t \left\| \hat{\boldsymbol{\omega}}_{rel,k-1} \right\|}{2} \right) \mathbb{I}_{4\times 4} + \frac{1}{\left\| \hat{\boldsymbol{\omega}}_{rel,k-1} \right\|} \sin\left(\frac{\Delta t \left\| \hat{\boldsymbol{\omega}}_{rel,k-1} \right\|}{2} \right) \left[\hat{\boldsymbol{\omega}}_{rel,k-1} \otimes \right] \right] \hat{\boldsymbol{q}}_{k-1} \\
\hat{\boldsymbol{\omega}}_{k} &= \hat{\boldsymbol{\omega}}_{k-1} - \Delta t J^{-1} \left(\left(J \hat{\boldsymbol{\omega}}_{k-1} \right) \times \hat{\boldsymbol{\omega}}_{k-1} \right) \\
\hat{b}_{j,k} &= \exp\left(-{}^{\Delta t}/_{\tau_j} \right) \hat{b}_{j,k-1}
\end{aligned} \tag{31}$$

where $\Delta t = t_{k} - t_{k-1}$, $\hat{\boldsymbol{\omega}}_{rel,k} = \hat{\boldsymbol{\omega}}^{VV}_{VV/RVN,k} = \hat{\boldsymbol{\omega}}^{VV}_{VV/ECI,k} - R\left(\hat{\boldsymbol{q}}_{VV/RVN,k} \right) \hat{\boldsymbol{\omega}}^{RVN}_{RVN/ECI,k}$, and the quaternion integration rule is derived by Markley.[25,4]

SYSTEM LINEARIZATION

While the Raven RNF uses the (approximate) nonlinear system dynamics to propagate the system state between measurement updates, the RNF uses the usual Extended Kalman Filter concept of using a linearized state dynamics model to propagate the state covariance as well as perform measurement updates.[26] The technique of using a three element error parameterization to derive linear dynamics for the quaternion state are based off the pioneering work of Lefferts, Markley, and Shuster[2,3,4] commonly known as the Multiplicative Extended Kalman Filter (MEKF).

The linearized error states for the translation nonlinear states are defined as:

$$\begin{aligned}
\Delta \boldsymbol{r} &= \boldsymbol{r} - \hat{\boldsymbol{r}} \\
\Delta \boldsymbol{v} &= \boldsymbol{v} - \hat{\boldsymbol{v}}
\end{aligned} \tag{32}$$

Taking the time derivative and substituting in the nonlinear dynamics equations, we find

$$\begin{aligned}
\Delta \dot{\boldsymbol{r}} &= \Delta \boldsymbol{v} \\
\Delta \dot{\boldsymbol{v}} &= -2\hat{\boldsymbol{\omega}}^{RVN}_{RVN/ECI} \times \Delta \boldsymbol{v} + W_{tran} \boldsymbol{w}_{tran}
\end{aligned} \tag{33}$$

The linearized error states for the rotation nonlinear states are defined as:

$$\begin{aligned}
\Delta \boldsymbol{g}\left(\Delta \boldsymbol{q} \right) &= \boldsymbol{g}\left(\boldsymbol{q} \otimes \hat{\boldsymbol{q}}^{-1} \right) \\
\Delta \boldsymbol{\omega} &= \boldsymbol{\omega} - R\left(\Delta \boldsymbol{q}^{-1} \right) \hat{\boldsymbol{\omega}}
\end{aligned} \tag{34}$$

The dynamics associated with the angular rate error state follow by computing the first order approximation of the Taylor series approximation of the derivative of the angular rate error state:[27]

$$\begin{aligned}\Delta\dot{\boldsymbol{\omega}} &\approx \frac{\partial}{\partial X}\left(\begin{matrix}^{ECI}\\ \end{matrix}\frac{d}{dt}\boldsymbol{\omega}_{VV/ECI}^{VV}\right)\Bigg|_{\mathbf{X}=\hat{\mathbf{X}}}\Delta\boldsymbol{x} + W_{rot}\boldsymbol{w}_{rot}\\ &= J^{-1}\left(\left[\left(J\hat{\boldsymbol{\omega}}\right)\times\right] - \left[\hat{\boldsymbol{\omega}}\times\right]J\right)\Delta\boldsymbol{\omega} + W_{rot}\boldsymbol{w}_{rot}\end{aligned} \tag{35}$$

The kinematics associated with the rotation error state are less straightforward to determine. First, we find the derivative of the error quaternion:

$$\Delta\dot{\boldsymbol{q}} = \dot{\boldsymbol{q}}\otimes\hat{\boldsymbol{q}}^{-1} + \boldsymbol{q}\otimes\frac{d}{dt}\left(\hat{\boldsymbol{q}}^{-1}\right) \tag{36}$$

The kinematic relation for the true relative quaternion was found in Equation 28 repeated here:

$$\dot{\boldsymbol{q}} = \frac{1}{2}\boldsymbol{\omega}_{VV/ECI}^{VV}\otimes\boldsymbol{q} - \frac{1}{2}\boldsymbol{q}\otimes\boldsymbol{\omega}_{RVN/ECI}^{RVN}$$

The kinematic relation for the estimated relative quaternion is merely the expectation of the above:

$$\dot{\hat{\boldsymbol{q}}} = \frac{1}{2}\hat{\boldsymbol{\omega}}_{VV'/ECI}^{VV'}\otimes\hat{\boldsymbol{q}} - \frac{1}{2}\hat{\boldsymbol{q}}\otimes\hat{\boldsymbol{\omega}}_{RVN/ECI}^{RVN} \tag{37}$$

A relation for $\frac{d}{dt}\left(\hat{\boldsymbol{q}}^{-1}\right)$ is found using the same technique as in Equation 27, yielding:

$$\frac{d}{dt}\left(\hat{\boldsymbol{q}}^{-1}\right) = -\frac{1}{2}\hat{\boldsymbol{q}}^{-1}\otimes\hat{\boldsymbol{\omega}}_{VV'/ECI}^{VV'} + \frac{1}{2}\hat{\boldsymbol{\omega}}_{RVN/ECI}^{RVN}\otimes\hat{\boldsymbol{q}}^{-1} \tag{38}$$

Substituting this result into Equation 36 yields

$$\begin{aligned}\Delta\dot{\boldsymbol{q}} &= \frac{1}{2}\boldsymbol{\omega}_{VV/ECI}^{VV}\otimes\boldsymbol{q}\otimes\hat{\boldsymbol{q}}^{-1} - \frac{1}{2}\hat{\boldsymbol{q}}\otimes\boldsymbol{\omega}_{RVN/ECI}^{RVN}\otimes\hat{\boldsymbol{q}}^{-1} - \frac{1}{2}\boldsymbol{q}\otimes\hat{\boldsymbol{q}}^{-1}\otimes\hat{\boldsymbol{\omega}}_{VV'/ECI}^{VV'} + \frac{1}{2}\boldsymbol{q}\otimes\hat{\boldsymbol{\omega}}_{RVN/ECI}^{RVN}\otimes\hat{\boldsymbol{q}}^{-1}\\ &= \frac{1}{2}\boldsymbol{\omega}_{VV/ECI}^{VV}\otimes\Delta\boldsymbol{q} - \frac{1}{2}\Delta\boldsymbol{q}\otimes\hat{\boldsymbol{\omega}}_{VV'/ECI}^{VV'}\\ &= \frac{1}{2}\boldsymbol{\omega}_{VV/ECI}^{VV}\otimes\Delta\boldsymbol{q} - \frac{1}{2}\Delta\boldsymbol{q}\otimes\Delta\boldsymbol{q}^{-1}\otimes\hat{\boldsymbol{\omega}}_{VV'/ECI}^{VV}\otimes\Delta\boldsymbol{q}\\ &= \frac{1}{2}\left(\boldsymbol{\omega}_{VV/ECI}^{VV} - \hat{\boldsymbol{\omega}}_{VV'/ECI}^{VV}\right)\otimes\Delta\boldsymbol{q}\\ &= \frac{1}{2}\left(\boldsymbol{\omega} - R\left(\Delta\boldsymbol{q}^{-1}\right)\hat{\boldsymbol{\omega}}\right)\otimes\Delta\boldsymbol{q}\\ &= \frac{1}{2}\Delta\boldsymbol{\omega}\otimes\Delta\boldsymbol{q}\end{aligned} \tag{39}$$

where we have assumed that the estimate $\hat{\boldsymbol{\omega}}_{RVN/ECI}^{RVN}$ from the Attitude Estimation Filter has negligible error.

By letting $\Delta \boldsymbol{q} = \begin{bmatrix} \Delta \boldsymbol{\epsilon} \\ \Delta \eta \end{bmatrix}$, we can re-write Equation 39 as

$$\Delta \dot{\boldsymbol{q}} = \begin{bmatrix} \Delta \dot{\boldsymbol{\epsilon}} \\ \Delta \dot{\eta} \end{bmatrix} = \frac{1}{2} \begin{bmatrix} \Delta \eta \Delta \boldsymbol{\omega} - \Delta \boldsymbol{\omega} \times \Delta \boldsymbol{\epsilon} \\ -\Delta \boldsymbol{\omega}^{T} \Delta \boldsymbol{\epsilon} \end{bmatrix} \tag{40}$$

We can now use the definition of the Gibbs parameters from Equation 13 and the relationships in Equation 40 to find the needed Gibbs error kinematics:

$$\begin{aligned} \Delta \dot{\boldsymbol{g}} &= \frac{\Delta \dot{\boldsymbol{\epsilon}} \Delta \eta - \Delta \dot{\eta} \Delta \boldsymbol{\epsilon}}{\Delta \eta^{2}} \\ &= \frac{\Delta \eta \Delta \boldsymbol{\omega} - \Delta \boldsymbol{\omega} \times \Delta \boldsymbol{\epsilon}}{2 \Delta \eta} + \frac{\Delta \boldsymbol{\omega}^{T} \Delta \boldsymbol{\epsilon} \Delta \boldsymbol{\epsilon}}{2 \Delta \eta^{2}} \\ &= \frac{1}{2} \Delta \boldsymbol{\omega} - \frac{1}{2} \Delta \boldsymbol{\omega} \times \Delta \boldsymbol{g} + \frac{1}{2} \Delta \boldsymbol{\omega}^{T} \Delta \boldsymbol{g} \Delta \boldsymbol{g} \\ &\approx \frac{1}{2} \Delta \boldsymbol{\omega} - \frac{1}{2} \Delta \boldsymbol{\omega} \times \Delta \boldsymbol{g} \end{aligned} \tag{41}$$

where we neglect terms that are second order in $\Delta \boldsymbol{g}$.

Finally, we define the error states associated with the sensor biases. The error state for bias j is defined simply as

$$\Delta b_{j} = b_{j} - \hat{b}_{j} \tag{42}$$

which obeys the following differential equation

$$\Delta \dot{b}_{j} = -\frac{1}{\tau_{j}} \Delta \dot{b}_{j} + \sigma_{j} w_{j} \tag{43}$$

The error equations can be combined in matrix form:

$$\begin{aligned} \Delta \dot{\boldsymbol{x}} &= \begin{bmatrix} \Delta \dot{\boldsymbol{r}} \\ \Delta \dot{\boldsymbol{v}} \\ \Delta \dot{\boldsymbol{g}} \\ \Delta \dot{\boldsymbol{\omega}} \\ \Delta \dot{\boldsymbol{b}} \end{bmatrix} = \begin{bmatrix} F_{tran} & 0_{6\times6} & 0_{6\times18} \\ 0_{6\times6} & F_{rot} & 0_{6\times18} \\ 0_{18\times6} & 0_{18\times6} & F_{b} \end{bmatrix} \begin{bmatrix} \Delta \boldsymbol{r} \\ \Delta \boldsymbol{v} \\ \Delta \boldsymbol{g} \\ \Delta \boldsymbol{\omega} \\ \Delta \boldsymbol{b} \end{bmatrix} + \begin{bmatrix} 0_{3\times3} & 0_{3\times3} & 0_{3\times18} \\ W_{tran} & 0_{3\times3} & 0_{3\times18} \\ 0_{3\times3} & 0_{3\times3} & 0_{3\times18} \\ 0_{3\times3} & W_{rot} & 0_{3\times18} \\ 0_{3\times3} & 0_{3\times3} & W_{b} \end{bmatrix} \begin{bmatrix} \boldsymbol{w}_{tran} \\ \boldsymbol{w}_{rot} \\ \boldsymbol{w}_{b} \end{bmatrix} \\ &= F \Delta \boldsymbol{x} + W \boldsymbol{w} \end{aligned} \tag{44}$$

where

$$F_{tran} = \begin{bmatrix} 0_{3\times3} & \mathbb{I}_{3\times3} \\ 0_{3\times3} & -2 \left[\hat{\boldsymbol{\omega}}^{RVN}_{RVN/ECI} \times \right] \end{bmatrix}$$

$$F_{rot} = \begin{bmatrix} -[\hat{\boldsymbol{\omega}} \times] & \frac{1}{2}\mathbb{I}_{3\times3} \\ 0_{3\times3} & J^{-1}\left([(J\hat{\boldsymbol{\omega}})\times] - [\hat{\boldsymbol{\omega}}\times]\, J\right) \end{bmatrix}$$

and $F_b = -\text{diag}\left(\frac{1}{\tau_1}, \frac{1}{\tau_2}, \ldots, \frac{1}{\tau_{18}}\right)$.

The state transition matrix can be approximated as

$$\begin{aligned} \Phi_k = \Phi\left(\Delta t_k\right) &= \mathbb{I} + \Delta t_k F_k + \frac{\Delta t_k^{\,2}}{2!} F_k^{\,2} + \ldots \\ &\approx \mathbb{I} + F\Delta t \\ &= \begin{bmatrix} \Phi_{tran,k} & 0_{6\times6} & 0_{6\times18} \\ 0_{6\times6} & \Phi_{rot,k} & 0_{6\times18} \\ 0_{18\times6} & 0_{18\times6} & \Phi_{b,k} \end{bmatrix} \end{aligned} \tag{45}$$

where

$$\Phi_{tran,k} = \begin{bmatrix} \mathbb{I}_{3\times3} & \Delta t_k \mathbb{I}_{3\times3} \\ 0_{3\times3} & \mathbb{I}_{3\times3} - 2\Delta t_k \left[\hat{\boldsymbol{\omega}}^{RVN}_{RVN/ECI} \times\right] \end{bmatrix}$$

$$\Phi_{rot,k} = \begin{bmatrix} \mathbb{I}_{3\times3} - \Delta t_k \left[\hat{\boldsymbol{\omega}}_k \times\right] & \frac{\Delta t_k}{2}\mathbb{I}_{3\times3} \\ 0_{3\times3} & \mathbb{I}_{3\times3} + \Delta t_k J^{-1}\left(\left[\left(J\hat{\boldsymbol{\omega}}_k\right)\times\right] - \left[\hat{\boldsymbol{\omega}}_k \times\right] J\right) \end{bmatrix}$$

and the exact solution for the bias error states' block of the state transition matrix is diagonal with the j^{th} bias's contribution expressed as $\left[\Phi_{b,k}\right]_{j,j} = \exp\left(-\Delta t_k / \tau_j\right)$.

The process noise matrix may now be approximated[26]

$$\begin{aligned} Q_k = Q\left(\Delta t_k\right) &= E\left\{ \left[\int_{t_{k-1}}^{t_k} \Phi\left(t_k - \epsilon\right) W \boldsymbol{w}(\epsilon) d\epsilon\right] \left[\int_{t_{k-1}}^{t_k} \Phi\left(t_k - \eta\right) W \boldsymbol{w}(\eta) d\eta\right]^T \right\} \\ &\approx \begin{bmatrix} Q_{tran,k} & 0_{6\times6} & 0_{6\times18} \\ 0_{6\times6} & Q_{rot,k} & 0_{6\times18} \\ 0_{18\times6} & 0_{18\times6} & Q_{b,k} \end{bmatrix} \end{aligned} \tag{46}$$

where

$$
\begin{aligned}
Q_{tran,k} &= \begin{bmatrix} \frac{\Delta t_k^{\,3}}{3} W_{tran} W_{tran}^{\,T} & Q_{tran,k,21} \\ Q_{tran,k,12} & Q_{tran,k,22} \end{bmatrix} \\
Q_{tran,k,21} &= \frac{\Delta t_k^{\,2}}{2} W_{tran} W_{tran}^{\,T} + \frac{2\Delta t_k^{\,3}}{3} W_{tran} W_{tran}^{\,T} \left[\hat{\boldsymbol{\omega}}^{\,RVN}_{RVN/ECI,k} \times \right] \\
Q_{tran,k,12} &= \frac{\Delta t_k^{\,2}}{2} W_{tran} W_{tran}^{\,T} - \frac{2\Delta t_k^{\,3}}{3} \left[\hat{\boldsymbol{\omega}}^{\,RVN}_{RVN/ECI,k} \times \right] W_{tran} W_{tran}^{\,T} \\
Q_{tran,k,22} &= \Delta t_k^{\,2} W_{tran} W_{tran}^{\,T} \left[\hat{\boldsymbol{\omega}}^{\,RVN}_{RVN/ECI,k} \times \right] - \Delta t_k^{\,2} \left[\hat{\boldsymbol{\omega}}^{\,RVN}_{RVN/ECI,k} \times \right] W_{tran} W_{tran}^{\,T} \\
&\quad + \Delta t_k W_{tran} W_{tran}^{\,T} - \frac{4\Delta t_k^{\,3}}{3} \left[\hat{\boldsymbol{\omega}}^{\,RVN}_{RVN/ECI,k} \times \right] W_{tran} W_{tran}^{\,T} \left[\hat{\boldsymbol{\omega}}^{\,RVN}_{RVN/ECI,k} \times \right]
\end{aligned}
$$

$$
\begin{aligned}
Q_{rot,k} &= \begin{bmatrix} \frac{\Delta t_k^{\,3}}{12} W_{rot} W_{rot}^{\,T} & \frac{\Delta t_k^{\,2}}{4} W_{rot} W_{rot}^{\,T} + \frac{\Delta t_k^{\,3}}{6} W_{rot} W_{rot}^{\,T} C_k^{\,T} \\ \frac{\Delta t_k^{\,2}}{4} W_{rot} W_{rot}^{\,T} + \frac{\Delta t_k^{\,3}}{6} C_k W_{rot} W_{rot}^{\,T} & Q_{rot,k,22} \end{bmatrix} \\
Q_{rot,k,22} &= t_k W_{rot} W_{rot}^{\,T} + \frac{\Delta t_k^{\,2}}{2} \left(W_{rot} W_{rot}^{\,T} C_k^{\,T} + C_k W_{rot} W_{rot}^{\,T} \right) + \frac{\Delta t_k^{\,3}}{3} C_k W_{rot} W_{rot}^{\,T} C_k^{\,T} \\
C_k &= J^{-1} \left(\left[\left(J \hat{\boldsymbol{\omega}}_k \right) \times \right] - \left[\hat{\boldsymbol{\omega}}_k \times \right] J \right)
\end{aligned}
$$

and the $Q_{b,k}$ block is diagonal with the $j^{\,th}$ bias's contribution expressed as

$$
\left[Q_{b,k} \right]_{j,j} = \frac{\tau_j \sigma_j^{\,2}}{2} \left(1 - \exp\left(-2^{\Delta t_k} / _{\tau_j} \right) \right)
$$

Using the state transition matrix and process noise matrix, the filter can now propagate the state covariance estimate between the measurement update at time t_{k-1} and the measurement update at time t_k using the standard EKF covariance propagation equation:[26]

$$
P_k^{\,-} = \Phi_k P_{k-1}^{\,+} \Phi_k^{\,T} + Q_k \tag{47}
$$

where the covariance matrix $P = E\left[\Delta \boldsymbol{x} \Delta \boldsymbol{x}^{\,T} \right]$, a negative symbol in the post-superscript indicates just before a measurement update (a-priori), and a positive symbol in the post-superscript indicates just after a measurement update (a-posteriori).

Note that the linearized error states do not need to be propagated. As is the case for a standard Extended Kalman Filter,[26,4] any information in the linearized error states is transferred to the full nonlinear states at the conclusion of a measurement update; after the information transfer, the linearized error states are "reset" to zero.[3] In other words, any information that the filter has about the system is incorporated into its estimate of the system state.

MEASUREMENT PROCESSING

Measurements from each of the vision algorithms GNFIR-VIS, GNFIR-IR, and FPOSE are pose measurements, consisting of a relative translation and relative orientation, denoted as $\left(\tilde{\boldsymbol{r}}^{\ VV}_{VV/RVN}, \tilde{\boldsymbol{q}}_{VV'/RVN}\right)$.

Measurement Models

The relative translation measurements are modeled as

$$\tilde{\boldsymbol{r}}^{\ VV}_{VV/RVN,CAM} = \boldsymbol{r}^{\ VV}_{VV/RVN} + \boldsymbol{b}_{CAM,tran} + M_{CAM,tran}\boldsymbol{m}_{CAM,tran} \tag{48}$$

where the measurement from CAM (either GNFIR-VIS, GNFIR-IR, of FPOSE) is corrupted by a first order Gauss Markov bias $\boldsymbol{b}_{CAM,tran}$ (whose dynamics are listed in Equation 16) and additive measurement noise $M_{CAM,tran}\boldsymbol{m}_{CAM,tran} \sim \mathcal{N}\left(\boldsymbol{0}, M_{CAM,tran}M^{T}_{CAM,tran}\right)$ which is a zero mean Gaussian white noise process. The relative translation portion of the measurement innovation is thus given by

$$\begin{aligned}
\Delta\boldsymbol{r}^{\ innov}_{CAM} &= \tilde{\boldsymbol{r}}^{\ VV}_{VV/RVN,CAM} - \hat{\boldsymbol{r}} - \hat{\boldsymbol{b}}_{CAM} \\
&= \boldsymbol{r}^{\ VV}_{VV/RVN} + \boldsymbol{b}_{CAM,tran} + M_{CAM,tran}\boldsymbol{m}_{CAM,tran} - \hat{\boldsymbol{r}} - \hat{\boldsymbol{b}}_{CAM} \\
&= \Delta\boldsymbol{r} + \Delta\boldsymbol{b}_{CAM,tran} + M_{CAM,tran}\boldsymbol{m}_{CAM,tran}
\end{aligned} \tag{49}$$

Relative orientation measurements are modeled as

$$\tilde{\boldsymbol{q}}_{VV'/RVN} = \boldsymbol{q}\left(\boldsymbol{b}_{CAM,rot} + M_{CAM,rot}\boldsymbol{m}_{CAM,rot}\right) \otimes \boldsymbol{q}_{VV/RVN} \tag{50}$$

where, as before, the measurement from CAM (either GNFIR-VIS, GNFIR-IR, or FPOSE) is corrupted by a first order Gauss Markov bias $\boldsymbol{b}_{CAM,rot}$ (whose dynamics are listed in Equation 16) and measurement noise $M_{CAM,rot}\boldsymbol{m}_{CAM,rot} \sim \mathcal{N}\left(\boldsymbol{0}, M_{CAM,rot}M^{T}_{CAM,rot}\right)$ which is a zero mean Gaussian white noise process. The relative orientation portion of the measurement innovation is given by

$$\begin{aligned}
\Delta\boldsymbol{q}^{\ innov}_{CAM} &= \boldsymbol{q}^{-1}\left(\hat{\boldsymbol{b}}_{CAM,rot}\right) \otimes \tilde{\boldsymbol{q}}_{VV'/RVN} \otimes \hat{\boldsymbol{q}}^{-1}_{VV/RVN} \\
&= \boldsymbol{q}^{-1}\left(\hat{\boldsymbol{b}}_{CAM,rot}\right) \otimes \boldsymbol{q}\left(\boldsymbol{b}_{CAM,rot} + M_{CAM,rot}\boldsymbol{m}_{CAM,rot}\right) \otimes \boldsymbol{q}_{VV/RVN} \otimes \hat{\boldsymbol{q}}^{-1}_{VV/RVN} \\
&= \boldsymbol{q}^{-1}\left(\hat{\boldsymbol{b}}_{CAM,rot}\right) \otimes \boldsymbol{q}\left(\boldsymbol{b}_{CAM,rot} + M_{CAM,rot}\boldsymbol{m}_{CAM,rot}\right) \otimes \Delta\boldsymbol{q}
\end{aligned} \tag{51}$$

Finally, making small angle assumptions and converting to a Gibbs parameterization using Equation 13, we find the innovation to be

$$\Delta\boldsymbol{g}^{\ innov}_{CAM} = \boldsymbol{g}\left(\Delta\boldsymbol{q}^{\ innov}\right) \approx \Delta\boldsymbol{g} - \Delta\boldsymbol{b} + M_{CAM,rot}\boldsymbol{m}_{CAM,rot} \tag{52}$$

Thus for a GNFIR-VIS measurement, the measurement partial matrix is given by

$$H_{VIS} = \begin{bmatrix} \mathbb{I}_{3\times3} & 0_{3\times3} & 0_{3\times3} & 0_{3\times3} & \mathbb{I}_{3\times3} & 0_{3\times3} & 0_{3\times12} \\ 0_{3\times3} & 0_{3\times3} & \mathbb{I}_{3\times3} & 0_{3\times3} & 0_{3\times3} & -\mathbb{I}_{3\times3} & 0_{3\times12} \end{bmatrix} \tag{53}$$

with an associated measurement noise matrix given as

$$R_{_{VIS}} = \begin{bmatrix} M_{_{VIS,tran}} M_{_{VIS,tran}}^{^T} & 0_{_{3\times3}} \\ 0_{_{3\times3}} & M_{_{VIS,rot}} M_{_{VIS,rot}}^{^T} \end{bmatrix} \tag{54}$$

The measurement partial matrices and noise matrices for the GNFIR-IR and FPOSE measurements are similar.

Measurement Update

The measurement update process for the Raven RNF closely follows that of the classic MEKF.[2,3] The procedure is detailed below in Algorithm 1 for a GNFIR-VIS measurement; the procedure is similar for measurements from the other sensor types. The procedure may benefit from more numerically stable mechanizations such as square root or UDU implementations, measurement editing (outlier removal), and underweighting[28] which, for the sake of brevity, are not discussed here.

Note that there is an observability issue in this formulation. Namely, the full state is not instantaneously observable. Even worse, the relative motion dynamics lack sufficient richness to provide excitation over time (for practical purposes, at least) without inclusion of orbital dynamics. In other words, the filter can not simultaneously solve for the relative pose as well as a bias from every relative pose sensor as there are infinitely many solutions. This issue manifests itself as error in the filter "sloshing" between the relative pose estimates and sensor bias estimates.

A simple solution to this issue is to use a consider Kalman filter implementation[29,30,26] (also known as a Schmidt Kalman filter) to prevent the filter from updating a portion of the state estimate. With this type of mechanization, the filter can "consider" (but not update) the bias states associated with one sensor but solve for all the others. This solution is instantaneously observable. For example, one may wish to "consider" the bias states associated with the most accurate sensor; the filter will then solve for the bias states of the other sensors. The solved-for bias states will absorb the offset between the various sensors' measurements relative to the most accurate sensor, whether those offsets are due to mechanical misalignment or computer vision algorithm errors. As these types of slowly varying pose measurement offsets have been observed in the operation of the GNFIR and FPOSE applications,[22] this solution provides an excellent mechanism to fuse the measurements.

The measurement update procedure may be used for a consider Kalman filter by simply zeroing the rows of the Kalman gain matrix associated with the states to be considered. Of course, more elegant implementations of the consider Kalman filter are available.[29,30,26] The consider state mechanization has recently been derived for a UDU filter.[31]

CONCLUSION

A Relative Navigation Filter was derived for the Raven ISS hosted payload. The navigation filter was based on a Multiplicative Extended Kalman Filter suitably modified to estimate relative translation and orientation. The rotation of both Raven and the visiting vehicle were explicitly taken into account. The filter state was augmented with sensor biases to provide a mechanism for the filter to "learn" the disparity between differing pose measurement sensors, a significant issue when using computer vision techniques

Compute Measurement Innovation

$$\Delta \boldsymbol{r}_{VIS}^{innov} = \tilde{\boldsymbol{r}}_{VIS} - \hat{\boldsymbol{r}}_{k}^{-} - \hat{\boldsymbol{b}}_{VIS,tran,k}^{-}$$

$$\Delta \boldsymbol{q}_{VIS}^{innov} = \boldsymbol{q}^{-1}\left(\hat{\boldsymbol{b}}_{VIS,rot,k}^{-}\right) \otimes \tilde{\boldsymbol{q}}_{VIS} \otimes \left(\hat{\boldsymbol{q}}_{k}^{-}\right)^{-1} = \begin{bmatrix} \Delta \boldsymbol{\epsilon}_{VIS}^{innov} \\ \Delta \eta_{VIS}^{innov} \end{bmatrix}$$

$$\Delta \boldsymbol{g}_{VIS}^{innov} = \boldsymbol{g}\left(\Delta \boldsymbol{q}_{VIS}^{innov}\right) = \frac{\Delta \boldsymbol{\epsilon}_{VIS}^{innov}}{\Delta \eta_{VIS}^{innov}}$$

Compute Kalman Gain

$$K_{k} = P_{k}^{-} H_{VIS}^{T}\left(H_{vis} P_{k}^{-} H_{VIS}^{T} + R_{VIS}\right)^{-1}$$

Update Covariance

$$P_{k}^{+} = \left(\mathbb{I}_{30\times 30} - K_{k} H_{VIS}\right) P_{k}^{-} \left(\mathbb{I}_{30\times 30} - K_{k} H_{VIS}\right)^{T} + K_{k} R_{VIS} K_{k}^{T}$$

Compute State Estimate Update

$$\Delta \boldsymbol{x}^{update} = \begin{bmatrix} \Delta \boldsymbol{r}^{update} \\ \Delta \boldsymbol{v}^{update} \\ \Delta \boldsymbol{g}^{update} \\ \Delta \boldsymbol{\omega}^{update} \\ \Delta \boldsymbol{b}^{update} \end{bmatrix} = K_{k} \begin{bmatrix} \Delta \boldsymbol{r}_{VIS}^{innov} \\ \Delta \boldsymbol{g}_{VIS}^{innov} \end{bmatrix}$$

Apply Update to State Estimate

$$\hat{\boldsymbol{r}}_{k}^{+} = \hat{\boldsymbol{r}}_{k}^{-} + \Delta \boldsymbol{r}^{update}$$

$$\hat{\boldsymbol{v}}_{k}^{+} = \hat{\boldsymbol{v}}_{k}^{-} + \Delta \boldsymbol{v}^{update}$$

$$\hat{\boldsymbol{q}}_{k}^{+} = \boldsymbol{q}\left(\Delta \boldsymbol{g}^{update}\right) \otimes \hat{\boldsymbol{q}}_{k}^{-}$$

$$\hat{\boldsymbol{\omega}}_{k}^{+} = \hat{\boldsymbol{\omega}}_{k}^{-} + \Delta \boldsymbol{\omega}^{update}$$

$$\hat{\boldsymbol{b}}_{k}^{+} = \hat{\boldsymbol{b}}_{k}^{-} + \Delta \boldsymbol{b}^{update}$$

Algorithm 1: Measurement Update Procedure for a GNFIR-VIS Pose Measurement.

applied to optical sensors that process dramatically different optical spectra. The filter mechanization was further altered to that of a consider mechanization (Schmidt Kalman filter) to solve observability issues.

ACKNOWLEDGMENTS

The authors would like to thank the help of Barrett Dillow, the advice of Russell Carpenter, the support of the Raven team, and the Spacecraft Servicing Capabilities Office. The Raven project would not be possible without the support of the United State's Department of Defense's Space Technology Program (DoD STP-H5).

REFERENCES

[1] S.-G. Kim, J. L. Crassidis, Y. Cheng, A. M. Fosbury, and J. L. Junkins, "Kalman Filtering for Relative Spacecraft Attitude and Position Estimation," *Journal of Guidance, Control, and Dynamics*, Vol. 30, No. 1, 2007, pp. 133–

143.

[2] E. J. Lefferts, F. L. Markley, and M. D. Shuster, "Kalman Filtering for Spacecraft Attitude Estimation," *Journal of Guidance, Control, and Dynamics*, Vol. 5, No. 5, 1982, pp. 417–429.

[3] F. L. Markley, "Attitude Error Representations for Kalman Filtering," *Journal of Guidance, Control, and Dynamics*, Vol. 26, No. 2, 2003, pp. 311–317.

[4] F. L. Markley and J. L. Crassidis, *Fundamentals of Spacecraft Attitude Determination and Control*, Vol. 33. Springer, 2014.

[5] L. Zhang, H. Yang, S. Zhang, H. Cai, and S. Qian, "Kalman Filtering for Relative Spacecraft Attitude and Position Estimation: a Revisit," *Journal of Guidance, Control, and Dynamics*, Vol. 37, No. 5, 2014, pp. 1706–1711.

[6] D. C. Woffinden and D. K. Geller, "Relative Angles-only Navigation and Pose Estimation for Autonomous Orbital Rendezvous," *Journal of Guidance, Control, and Dynamics*, Vol. 30, No. 5, 2007, pp. 1455–1469.

[7] N. Philip and M. Ananthasayanam, "Relative Position and Attitude Estimation and Control Schemes for the Final Phase of an Autonomous Docking Mission of Spacecraft," *Acta Astronautica*, Vol. 52, No. 7, 2003, pp. 511–522.

[8] L. Song, Z. Li, and X. Ma, "Autonomous Rendezvous and Docking of an Unknown Tumbling Space Target with a Monocular Camera," *Guidance, Navigation and Control Conference (CGNCC), 2014 IEEE Chinese*, IEEE, 2014, pp. 1008–1013.

[9] X. Tang, J. Wei, and K. Chen, "Square-root Adaptive Cubature Kalman Filter with Application to Spacecraft Attitude Estimation," *Information Fusion (FUSION), 2012 15th International Conference on*, IEEE, 2012, pp. 1406–1412.

[10] F. Yu, Z. He, B. Qiao, and X. Yu, "Stereo-Vision-Based Relative Pose Estimation for the Rendezvous and Docking of Noncooperative Satellites," *Mathematical Problems in Engineering*, Vol. 2014, 2014.

[11] Y. Xing, X. Cao, S. Zhang, H. Guo, and F. Wang, "Relative Position and Attitude Estimation for Satellite Formation with Coupled Translational and Rotational Dynamics," *Acta Astronautica*, Vol. 67, No. 3, 2010, pp. 455–467.

[12] B. E. Tweddle and A. Saenz-Otero, "Relative Computer Vision-Based Navigation for Small Inspection Spacecraft," *Journal of Guidance, Control, and Dynamics*, Vol. 38, No. 5, 2014, pp. 969–978.

[13] J. Stuelpnagel, "On the Parametrization of the Three-Dimensional Rotation Group," *SIAM review*, Vol. 6, No. 4, 1964, pp. 422–430.

[14] M. D. Shuster, "A Survey of Attitude Representations," *The Journal of the Astronautical Sciences*, Vol. 41, No. 4, 1993, pp. 439–517.

[15] P. Hughes, *Spacecraft Attitude Dynamics*. Courier Dover Publications, 2012.

[16] F. L. Markley, "Unit Quaternion from Rotation Matrix," *Journal of Guidance, Control, and Dynamics*, Vol. 31, No. 2, 2008, pp. 440–442.

[17] M. E. Pittelkau, "Rotation Vector in Attitude Estimation," *Journal of Guidance, Control, and Dynamics*, Vol. 26, No. 6, 2003, pp. 855–860.

[18] M. Strube, R. Henry, E. Skeleton, J. V. Eepoel, N. Gill, and R. McKenna, "Raven: An On-Orbit Relative Navigation Demonstration Using International Space Station Visiting Vehicles," *American Astronautical Society*, 2015.

[19] T. Drummond and R. Cipolla, "Real-Time Visual Tracking of Complex Structures," *IEEE Transactions on Pattern Analysis and Machine Intelligence*, 2002.

[20] B. J. Naasz, J. Van Eepoel, S. Z. Queen, C. Southward, I. Michael, and J. Hannah, "Flight Results from the HST SM4 Relative Navigation Sensor System," *Advances in the Astronautical Sciences*, Vol. 137, No. 58, 2010, p. 2010.

[21] P. J. Besl and N. D. McKay, "Method for Registration of 3-D Shapes," *Robotics-DL tentative*, International Society for Optics and Photonics, 1992, pp. 586–606.

[22] J. M. Galante, J. Van Eepoel, M. Strube, N. Gill, M. Gonzalez, A. Hyslop, and B. Patrick, "Pose Measurement Performance of the Argon Relative Navigation Sensor Suite in Simulated Flight Conditions," *AIAA Guidance, Navigation, and Control Conference*, 2012.

[23] W. Clohessy and R. Wiltshire, "Terminal Guidance System for Satellite Rendezvous," Vol. 8, No. 2, 1985, pp. 235–242.

[24] M. Farahmand, A. Long, and R. Carpenter, "Magnetospheric Multiscale Mission Navigation Performance Using the Goddard Enhanced Onboard Navigation System," *Proceeding of the 25th International Symposium of Space Flight Dynamics, Munich, Germany*, 2015.

[25] J. R. Wertz, *Spacecraft Attitude Determination and Control*. Boston, MA: Kluwer Academic Publishers, 1978.

[26] R. G. Brown and P. Y. Hwang, *Introduction to Random Signals and Applied Kalman Filtering*. New York, NY: John Wiley and Sons, 3rd ed., 1997.

[27] J. Thienel and F. L. Markley, "Comparison of Angular Velocity Estimation Methods for Spinning Spacecraft," *AIAA Guidance, Navigation, and Control Conference*, 2012, p. 6432.

[28] R. Zanetti, K. J. DeMars, and R. H. Bishop, "Underweighting Nonlinear Measurements," *Journal of guidance, control, and dynamics*, Vol. 33, No. 5, 2010, pp. 1670–1675.

[29] S. F. Schmidt, "Applications of State Space Methods to Navigation Problems," *Advances in Control Systems*, Vol. 3, 1966, pp. 293–340.

[30] A. H. Jazwinski, *Stochastic Processes and Filtering Theory*. Courier Corporation, 2007.

[31] R. Zanetti and C. DSouza, "Recursive Implementations of the Consider Filter," *Proceedings of the AAS Jer-Nan Juang Astrodynamics Symposium*, 2012.